Solid Freeform Fabrication 2017: Proceedings of the 28th Annual International Solid Freeform Fabrication Symposium – An Additive Manufacturing Conference
Reviewed Paper

Mechanical Assessment of a LPBF Nickel Superalloy using the Small Punch Test Method

S. J. Davies*, S. P. Jeffs*, R. J. Lancaster*, G. Baxter†.

*Institute of Structural Materials, Swansea University, Bay Campus, Fabian Way, Swansea, SA1 8EN, UK.
†Rolls-Royce plc; P.O. Box 31, Derby DE24 8BJ, UK.

Abstract

With the continuous drive of the aerospace industry to introduce Additive Layer Manufacturing (ALM) into next generation gas turbine engines, the requirement to understand their mechanical performance has grown. However, limitations in material availability due to the nature of the process can restrict the scope for conventional mechanical testing. The Small Punch Tensile (SPT) test provides an effective tool for ranking the performance of ALM processed alloys, credited to the small volumes of material utilised and the ability to sample localised regions. This technique has been applied to the nickel superalloy C263, manufactured via Laser Powder Bed Fusion (LPBF) in different build orientations and subjected to contrasting post process heat treatments. To fully understand the effects of these process variables on the mechanical response of LPBF alloys, empirical correlations have been derived between SPT and uniaxial data attempting to demonstrate the suitability of this approach in characterising the properties of ALM structures.

Introduction

Additive Layer Manufacturing (ALM) is now a widely recognised process that encompasses the family of innovative net-shape fabrication techniques involving the layer-by-layer consolidation of material with a high-energy heat source to build a three-dimensional product [1–4]. ALM is highly attractive to the aerospace industry over more conventional processing routes since it has the potential to provide improved lead times, the ability to improve geometric complexity and the benefit of reduced material wastage, which can result in an improved buy-to-fly ratio [5,6].

The Laser Powder Bed Fusion (LPBF) manufacturing process is a derivative of ALM, capable of producing fully-dense components by selectively melting two-dimensional layers in to a bed of metallic powders using a laser heat source within an inert environment. Between the solidification of each layer the powder bed is retracted and a new layer of powder is deposited [2,7], with this process repeating until the three-dimensional component is complete. It has been recognised that material manufactured via this route is sensitive to the process variables assigned to the build, including laser power, scanning speed, hatch spacing, powder layer thickness amongst several others [2,7]. Factors outside of process variables must be considered such as component geometries and build orientation since these can influence the final microstructure and subsequent mechanical properties [4,6]. Furthermore, the transient microstructures that are characteristic of ALM components, can lead to an anisotropic behaviour in such materials which may then necessitate the use of heat treatment procedures to alleviate such issues. Therefore, a sophisticated and systematic approach to mechanical testing is needed to fully understand the evolving properties across ALM structures and parts or where material volume is limited.

The Small Punch Tensile (SPT) test technique can be used as an effective tool for ranking the mechanical performance of LPBF alloys. The test primarily involves the biaxial deformation of a miniature disc providing load-displacement data [8]. First introduced in the power generation and nuclear industries to assess the remnant life of steel structures and ductility losses in nuclear reactors, the Small Punch (SP) test has since been applied to a range of materials under both static and variable loads to deliver a creep and tensile-like response respectively [9,10]. For ALM, the small volumes of material expended in each test is particularly beneficial, considering constraints in material availability, whilst the ability to extract specimens from discrete locations also allows for factors such as build height and geometry sensitivity to be evaluated [9]. However, one of the challenges of this test type is to convert the load-displacement relationship into more established mechanical properties such as yield strength and ultimate tensile strength (UTS), allowing

for direct comparisons with available uniaxial test data. Various methods have been employed attempting to correlate this information [8,11,12].

The aim of this study is to correlate SPT values with available uniaxial tensile data for cast and four LPBF variants of the nickel-based superalloy C263. LPBF C263 was built both vertically (90°) and horizontally (0°) and heat treated with one of two heat treatments, namely SHT1, a standard heat treatment for this alloy [4], and SHT2. The SHT2 was applied to alleviate anisotropy commonly found in ALM material, although uniaxial tensile data for this variation is unknown. The refinement of this correlation by testing these variants over a range of temperatures should demonstrate whether correlations are appropriate and aid in further understanding the mechanical response of LPBF C263, providing the ability to calculate yield strength and UTS values for variants where the uniaxial data is not available.

Experimental Procedures

SPT tests were performed on an in-house designed Nimonic-90 jig to provide sufficient clamping of the miniature disc specimen and alignment of the punch normal to the disc surface. An upper and lower die clamps the specimen, with the latter possessing a 4mm receiving hole. The specimen is then deformed by the 2.5mm diameter hemispherical punch under a constant rate of displacement, forcing the disc through the lower die receiving hole. Dimensions of the jig assembly all comply to the European Code of Practice (EUCoP) for Small Punch testing [13]. A linear variable displacement transducer (LVDT) maintains contact with the underside of the disc via a quartz rod to allow for intimate monitoring of disc deflection. Load is delivered by a servo-actuated electric screw uniaxial test machine which is in direct contact with the punch. A threaded cylindrical block houses the afore-mentioned components and fastens the jig assembly to the test machine, this setup is shown in Figure 1. Loads were applied to the miniature disc specimens at a $0.3mm \cdot min^{-1}$ displacement rate, falling within the bounds outlined by the EUCoP [13]. Elevated temperatures were delivered by a radiant furnace, together with two N-type thermocouples attached in the jig assembly to monitor specimen temperature, where the EUCoP recommends temperatures fall between $\pm 0.25\%$ of the test temperature in degrees absolute, K [13].

Figure 1 – SPT jig setup [6].

SP discs of LPBF variants were sectioned from the stub ends of uniaxial test pieces. The material was then turned down to Ø9.5mm to allow the extraction of discs of the same diameter. Cast discs were sectioned from Ø9.5 cylinders extracted from a larger cast C263 piece using Electrical Discharge Machining (EDM). In each instance, discs were prepared for testing by grinding to a thickness of $500\mu m \pm 5\mu m$ with silicon carbide abrasive papers, finishing with 1200 grit grade, in agreement with the EUCoP [13]. Microstructures on two perpendicular planes in relation to a uniaxial specimen of each C263 variant can be found in Figure 2. SHT1 variants display a columnar grain structure, orientated parallel to the build direction. This structure is also true for the SHT2 90° material, although not as prominent. For each of the LPBF tests, the punch is in direct contact normal to the microstructures present on the X-Z plane. Grain size measurements for each C263 material type were obtained by the mean linear intercept (MLI) method and are displayed in Table 1 [14]. Optical microscopy was performed with a Reichert Jung MeF3 optical microscope on polished specimens, swab etched at room temperature using Kallings 2 reagent (5 g CuCl2 + 100 ml HCl + 100 ml ethanol) as per ASTM E407 [15].

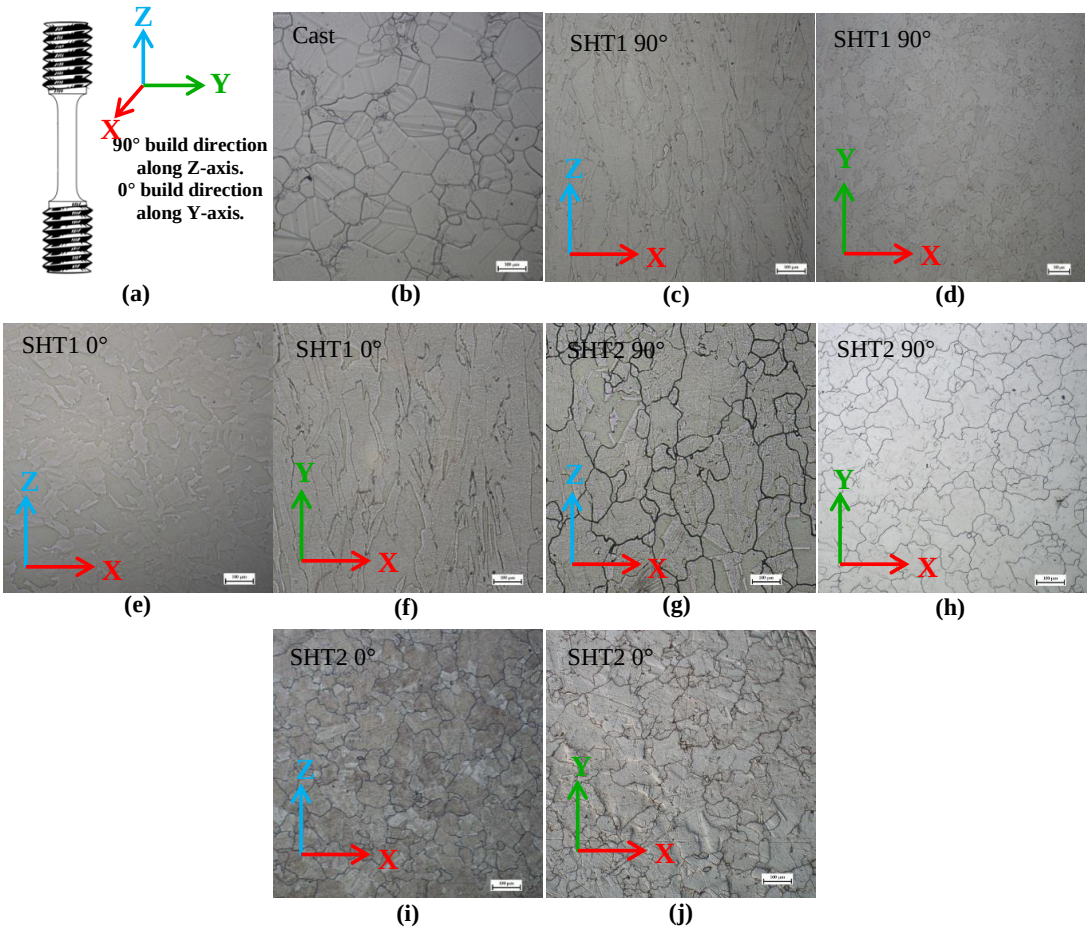

Figure 2 - (a) Schematic of build directions in relation to uniaxial specimens; (b-j) Micrographs of C263 variant microstructures on both the x-z and x-y plane [14].

Table 1 – C263 variant grain size measurements [14].

C263 Type	Average Equiaxed Grain Size (µm)	Average Columnar Grain Height (µm)	Average Columnar Grain Width (µm)
Cast	83	-	-
SHT1 90°	-	118	43
SHT1 0°	-	111	52
SHT2 90°	-	110	86
SHT2 0°	84	-	-

Results & Discussion

Figure 3a illustrates the typical load-displacement response of a ductile material subjected to the SPT test, in this case from a cast C263 disc specimen at 600°C. The literature suggests that the deformation of a SPT disc can be described by different deformation regions, namely elastic deformation, yield, plastic bending and membrane stretching until final necking to failure [8]. The elastic-plastic transition or yield load, F_e, and the peak load, F_m, are labelled on the load-displacement curve in Figure 3a, these properties will be the focus of the uniaxial correlations. Figure 4a demonstrates how the mechanical response of the

cast variant evolves as test temperature is increased. The peak loads and their respective displacements reduce as temperatures are increased up to 400°C. At 600°C the peak load and displacement significantly increases, followed by a dramatic deterioration when exposed to 780°C. Figure 4b shows the difference between each material variant at 20°C. All LPBF build variants exhibited a stronger response to the SPT test compared to the cast type, with the SHT1 variants displaying a higher displacement accumulated up to the peak load compared to all variants. Peak loads of the cast and SHT1 C263 types at each temperature are given in Table 2.

While the peak load on a SPT curve is simple to recognise, the accepted yield load is more difficult to obtain. Multiple methods of determining F_e have been proposed and has recently been the source of discussion [11,12]. However, it is a modification of the "two-secant method" which is preferred and recommended in the EUCoP, given in Equations 1-3 and presented in Figure 3b [13]. This involves a bi-linear fit on the load-displacement curve, limited up to where the displacement equates to the disc specimen thickness (0.5mm). After minimising the error between the bi-linear fit and the load-displacement plot (Equation 3), an intersection between the two linear functions is realised and the projection of this intersection point on the load-displacement curve is then considered to be the SP yield load, F_e [11–13]. This method has been applied to all C263 build variants to obtain yield load values. For the cast and SHT1 variants, these yield loads are recorded in Table 2 along with their respective peak load values.

$$0 \le u \le u_A \quad f(u) = \frac{f_A}{u_A} u, \tag{1}$$

$$u_A \le u \le u_B \quad f(u) = \frac{f_B - f_A}{u_B - u_A}(u - u_A) + f_A \tag{2}$$

$$err = \int_0^{u_B} [F(u) - f(u)]^2 du \tag{3}$$

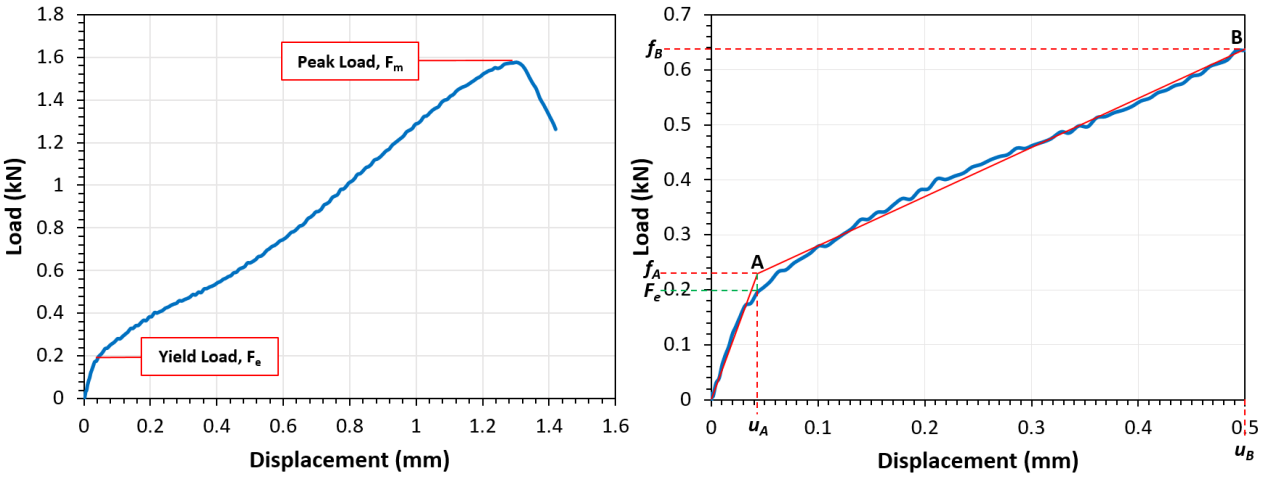

Figure 3 – (a) Typical SPT load displacement curve – cast C263 tested at 600°C; **(b)** Bi-linear function to determine F_e on a load-displacement curve [13].

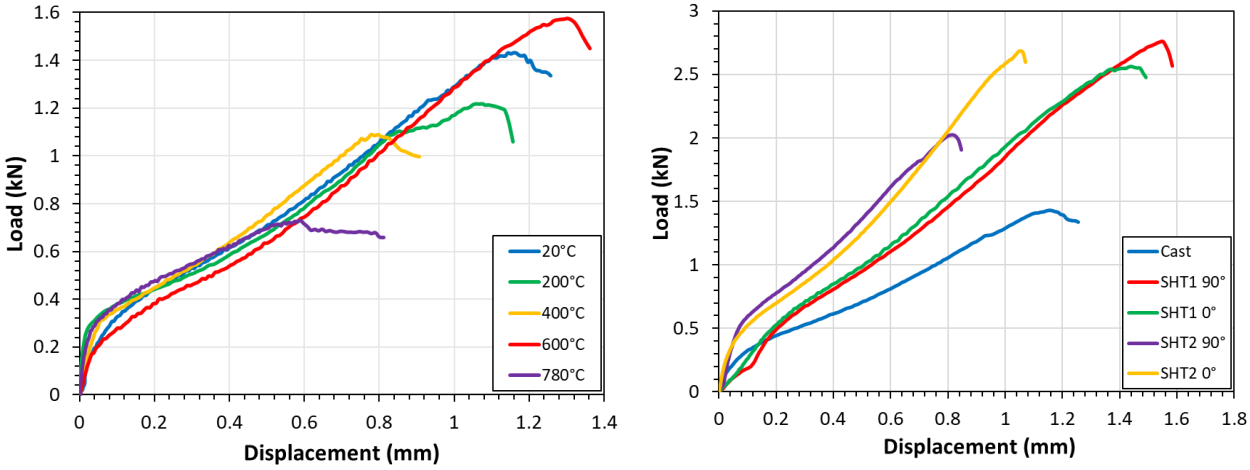

Figure 4 – (a) Load-displacement graph of cast material at each test temperature; **(b)** load-displacement graph of all material variants at 20°C.

Table 2 – Cast and SHT1 C263 data for SPT and uniaxial tests with SP effective stresses.

C263 Type	Temperature (°C)	F_e (kN)	Uniaxial Yield (MPa)	F_m (kN)	Uniaxial UTS (MPa)
Cast	20	0.306	430	1.454	620
	200	0.246	389	1.241	571
	300	0.282	375	1.663	554
	400	0.266	363	1.104	541
	600	0.197	349	1.598	517
	780	0.258	339	0.750	497
SHT1 90°	20	0.492	843*	2.798	1268*
	200	0.392	754	2.127	1051
	300	0.396	761	2.243	1018
	400	0.346	729	2.267	967
	780	0.243	431	0.422	548
SHT1 0°	20	0.523	709*	2.610	981*
	780	0.310	577	0.667	676

*Data from Vilaro et al. [4].

To correlate the determined SPT load values into effective stresses, empirical approaches need to be employed, summarised by Equations 4 and 5, demonstrating how values directly from the load-displacement curves can be used to calculate mechanical properties such as an effective yield strength (σ_y) and UTS (σ_{UTS}):

$$\sigma_y = \alpha_1 \frac{F_e}{h_0^2} + \alpha_2, \tag{4}$$

$$\sigma_{UTS} = \beta_1' \frac{F_m}{h_0^2} + \beta_2', \tag{5}$$

where, F_e, h_0, and F_m are the yield load, disc thickness and peak load respectively and parameters α_1, α_2, β_1' and β_2' are constants derived empirically by correlating SPT test results to their uniaxial data counterparts [11,12]. As well as the SPT loads, Table 2 also displays the available uniaxial tensile mechanical properties for the C263 variants. Through plotting F_e/h_0^2 and F_m/h_0^2 against the known uniaxial yield stress and UTS as displayed in Figure 5, the equation parameters are obtained. Previous research has shown that different values for these constants can be generated for different material types [11,12,16].

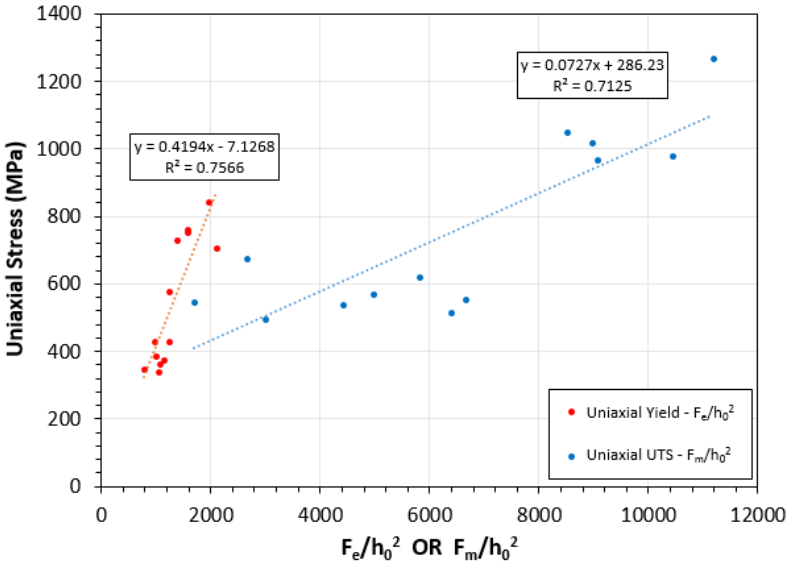

Figure 5 – Relationship between SPT and uniaxial data by plotting Yield Stress vs. F_e/h_0^2 and UTS vs. F_m/h_0^2 for Cast and SHT1 C263 variants.

The high R^2 values associated with these two relationships reveal there is a strong correlation between uniaxial and SPT mechanical responses for both cast and SHT1 LPBF C263 over the range of test conditions. The resulting correlations are displayed in equations 6 and 7:

$$\sigma_y = 0.4194\frac{F_e}{h_0^2} - 7.13, \tag{6}$$

$$\sigma_{UTS} = 0.0727\frac{F_m}{h_0^2} + 286.23. \tag{7}$$

Using equations 6 and 7, the effective yield strengths and UTS can be calculated for all C263 material variants, especially for those heat treated with SHT2 where prior uniaxial tensile test data is not known; these values are presented in Table 3. Although the generated parameters α_1, α_2, β_1' and β_2' are comparable to those quoted in the literature [11,12], the fact that they are not identical highlights the material dependency to this approach. Nevertheless, based on the effective strength values gained from this correlation, it has shown that this method has proved successful in providing mechanical property estimations for LPBF variants of C263. Furthermore, the establishment of these correlations allows for any future adjustments to the LPBF and post-process parameters to be characterised by the SPT method and provide estimated mechanical properties.

Table 3 – C263 SPT data with effective stresses and strength debits as a result of elevated temperatures.

C263 Type	Temperature (°C)	F_e (kN)	Effective Yield (MPa)	Yield Strength Debit (%)	F_m (kN)	Effective UTS (MPa)	UTS Debit (%)
Cast	20	0.306	506	15.9	1.454	709	28.9
	780	0.258	426		0.750	504	
SHT1 90°	20	0.492	818	51.1	2.798	1100	62.8
	780	0.243	401		0.422	409	
SHT1 0°	20	0.523	870	41.1	2.610	1045	54.1
	780	0.310	513		0.667	480	
SHT2 90°	20	0.507	843	42.0	2.063	886	33.5
	780	0.296	489		1.041	589	
SHT2 0°	20	0.356	590	49.2	2.724	1078	49.2
	780	0.268	442		0.901	548	

Although the rankings based on mechanical performance remain unchanged between each material variant, by calculating the effective yield and UTS, all C263 variants, including SHT2 LPBF types, can be analysed in terms of strength. It has been revealed that the cast variant had experienced a 16% reduction in yield strength when exposed to 780°C compared with its performance at 20°C, along with a 29% UTS deficit. This strength drop is relatively low compared to the LPBF SHT1 variants, displaying approximately a 41-51% drop in yield strength and a 54-63% reduction in UTS between the two build orientations resulting from exposure to the peak temperature condition. Build variants subjected to the SHT2 exhibited a decrease in yield strength of 42-49% and a reduction in UTS of 34-49% between the two build orientations. This strength retention at elevated temperature in SHT2 specimens is attributed to this increase in solution heat treatment temperature, when compared with the mechanical performance of SHT1 alloys. In each case the LPBF material is not competitive in terms of strength retention at elevated temperatures compared to cast variant. A thorough microstructural characterisation will be performed on each material variant to fully understand these outcomes as part of an ongoing study.

Conclusions

SPT tests at a range of temperatures have been carried out on cast and LPBF build variants of the nickel superalloy C263 to attain a parallel SP data-set alongside available uniaxial tensile results. This has allowed for correlations between the two test techniques to be deduced so traditional mechanical properties can be obtained from SPT load-displacement curves:

1. For each SPT test, the achieved peak loads have been extracted and the yield loads have been calculated using the modified "two-secant method" approach.
2. These peak and yield loads have been correlated with known uniaxial data for yield strength and UTS respectively over the range of C263 alloys, with strong correlations and equations parameters determined in each case. These equations have been used to calculate effective strength values for all alloy variant, even the SHT2 LPBF where uniaxial data was unavailable.
3. Effective yield and UTS values have been used to assess the effects of elevated temperatures in terms of strength deterioration across all build variants. Cast C263 had retained more of its strength from 20°C to 780°C compared with all LPBF variants. However, the introduction of SHT2 helped reduce the debit in strength seen in the SHT1 material after exposure to elevated temperatures.

Acknowledgements

The current research was funded under the EPSRC Rolls-Royce Strategic Partnership in Structural Metallic Systems for Gas Turbines (grants EP/H500383/1 and EP/H022309/1). The provision of materials and supporting information from Rolls-Royce plc are gratefully acknowledged by the authors. Mechanical tests were performed at Swansea Materials Research and Testing Ltd. (SMaRT).

References

[1] Antonysamy, A.A. Microstructure, Texture and Mechanical Property Evolution during Additive Manufacturing of Ti6Al4V Alloy for Aerospace Applications. 2012.

[2] Illston, T. Material Solutions-Additive Manufacturing. U.S. Patent Application No. US 2014/0034626 A1, 6 February 2014.

[3] Murr, L.E.; Gaytan, S.M.; Ramirez, D.A.; Martinez, E.; Hernandez, J.; Amato, K.N.; Shindo, P.W.; Medina, F.R.; Wicker, R.B. Metal Fabrication by Additive Manufacturing Using Laser and Electron Beam Melting Technologies. J. Mater. Sci. Technol. 2012, 28, 1–14.

[4] Vilaro, T.; Colin, C.; Bartout, J.D.; Nazé, L.; Sennour, M. Microstructural and Mechanical Approaches of the Selective Laser Melting Process Applied to a Nickel-Base Superalloy. Mater. Sci. Eng. A 2012, 534, 446–451.

[5] Carter, L.N.; Martin, C.; Withers, P.J.; Attallah, M.M. The Influence of the Laser Scan Strategy on Grain Structure and Cracking Behaviour in SLM Powder-Bed Fabricated Nickel Superalloy. J. Alloys Compd. 2014, 615, 338–347.

[6] Illsley, H.W; Lancaster, R.J; Hurst, R.C.; Jeffs, S.P., Small Punch Testing of Electron Beam Melted (EBM) Ti-6Al-4V. 2015.

[7] Gong, H.; Rafi, K.; Starr, T.; Stucker, B. The Effects of Processing Parameters on Defect Regularity in Ti-6Al-4V Parts Fabricated By Selective Laser Melting and Electron Beam Melting. In Proceedings of the 24th Annual International Solid Freeform Fabrication Symposium, Austin, TX, USA, 12–14 Augest 2013.

[8] Norris, S.D.; Parker, J.D. Deformation Processes During Disc Bend Loading. Mater. Sci. Technol. 1996, 12, 163–170.

[9] Lancaster, R.J.; Banik, R.; Hurst, R.C.; Bache, M.R.; Baxter, G. Application of Small Punch Test Methods to Advanced Manufactured Structures. In Proceedings of the 3rd International SSTT Conference: Determination of Mechanical Properties of Materials by Small Punch and other Miniature Testing Techniques, Schloss Seggau, Austria, 23–25 September 2014, 170–178.

[10] Jeffs, S.P.; Lancaster, R.J. Small Punch Creep Testing of Single Crystal Superalloys. In Proceedings of the 3rd International SSTT Conference: Determination of Mechanical Properties of Materials by Small Punch and other Miniature Testing Techniques, Schloss Seggau, Austria, 23–25 September 2014, 282–292.

[11] Bruchhausen, M.; Holmström, S. Recent Developments in Small Punch Testing: Tensile Properties and DBTT. Theor. Appl. Fract. Mech. 2016, 86, 2–10.

[12] García, T.E.; Rodríguez, C.; Belzunce, F.J.; Suárez, C. Estimation of the Mechanical Properties of Metallic Materials by means of the Small Punch Test. J. Alloys Compd. 2014, 582, 708–717.

[13] European Code of Practise: Small Punch Test Method for Metallic Materials; CEN Workshop Agreement, CWA 15267; CEN-European Committee for Standardization: Brussels, Belgium, 2007.

[14] Davies, S.J.; Jeffs, S.P.; Lancaster, R.J..; Baxter, G. High Temperature Deformation Mechanisms in a DLD Nickel Superalloy. *Materials* 2017, 10, 457.

[15] Standard Practice for Microetching Metals and Alloys; ASTM E407-07(2015)e; ASTM International: West Conshohocken, PA, USA, 2015.

[16] Dobeš, F.; Dymáˇcek, P.; Besterci, M. Estimation of the Mechanical Properties of Aluminium and an Aluminium Composite after Equal Channel Angular Pressing by means of the Small Punch Test. Mater. Sci. Eng. A 2015, 626, 313–321.